Hindawi
Complexity
Volume 2019, Article ID 1670284, 13 pages
https://doi.org/10.1155/2019/1670284

Research Article

Design, Modeling, and Experiments of the Vortex-Induced Vibration Piezoelectric Energy Harvester with Bionic Attachments

Zunlong Jin,[1,2] Guoping Li,[1,2] Junlei Wang ,[1,2] and Zhien Zhang [2]

[1]*School of Chemical Engineering and Energy, Zhengzhou University, Zhengzhou 450001, China*
[2]*Engineering Research Center of Energy Saving Technology and Equipment of Thermal Energy System, Ministry of Education, Zhengzhou 450001, China*

Correspondence should be addressed to Junlei Wang; just4pipi@126.com

Received 25 November 2018; Revised 12 January 2019; Accepted 17 March 2019; Published 4 April 2019

Academic Editor: Dimitri Volchenkov

Since the energy demand increases, the sources of fluid energy such as wind energy and marine energy have attracted widespread attention, especially vortex-induced vibrations excited by wind energy. It is well known that the lock-in effect in vortex-induced vibration can be applied to the piezoelectric energy harvester. Although numerous researches have been conducted on piezoelectric energy harvesting devices in recent years, a common problem of low bandwidth and harvesting efficiency still exists. In order to increase the response amplitude and decrease the threshold wind speed of vortex-induced vibration, a bionic attachment structure is proposed based on the experimental method. In the present work, twelve models are designed according to the size of pits and hemispheric protrusions which are added to the surface of a flexible smooth cylinder. Compared with the smooth cylinder which is taken as a carrier, the harvester with the bionic structure shows stronger energy capture performance on the whole. As the threshold speed decelerates from 1.8m/s to 1 m/s, the bandwidth, on the contrary, increases from 39.3% to 51.4%. Particularly, for the 10 mm pits structure with 5 columns, its peak voltage can reach 47 V, and its peak power can reach 1.21 mW with a resistance of 800 kΩ, 0.57 mW higher than that of the smooth cylinder. Comparatively speaking, the hemispherical projections structure figures with a much more different energy capturing characteristic. Starting from the column, the measured voltage of the hemispherical bionic harvester is much smaller than that of the smooth cylinder, with a peak voltage less than 15 V and a reducing bandwidth. However, compared with the smooth cylinder, hemispheric projections with 3 columns have a better energy capture effect with a measured voltage of 35V, a resistance of 800kΩ, and a wind speed of 3.097 m/s. Besides, its output power also enhances from 0.48 to 0.56 mW.

1. Introduction

Energy policy has become a key strategy in the recent decades in the world [1], and researches focus on energy has been extended in many fields, e.g., environmental protection [2–4], industrial catalysis [5–7], and energy storage [8–13]. Additionally, in recent years, under the background of big data technology [14, 15], some new types of low-power consumption technologies like MEMs and WSNs [16, 17] have been introduced into many areas. As a widespread phenomenon in the natural environment, fluid flow contains a lot of energy, which will provide great convenience for power systems to transform the kinetic energy of fluid into electricity, especially for those that need electronic components with lower power. Over the past few years, a new technology based on vortex-induced vibration has been widely developed to extract energy from wind and oceanic or other fluid flow energy; in brief, the source of energy is responsible for the vibration. Nevertheless, as a destructive phenomenon in the engineering structure for a long time, vortex-induced vibration requires a nonlinear bluff body structure such as a cylinder of smooth surface. In engineering, when the fluid flows through the surface of the bluff body [18–20], the flow will separate on the surface of the bluff body at the same time, and then the vortex begins to shed alternately around the bluff body under the action of the shear layer, thus generating periodic fluid force which will act on the surface of the cylinder. The bluff body begins to oscillate

when the frequency of the vortex shedding corresponds to the natural frequency of the elastic structural oscillations. As the fluid dynamics theory emerges, an effective drag reduction method called bionic drag reduction has been found, which can not only reduce the resistance, but also be widely used in energy collection. It is green, simple, and feasible for the bionic structure to extend the bandwidth and increase the voltage in the energy harvesting system. Since the last decade, the bionic structure drag reduction has become much more prevalent, motivating more and more scholars to do a lot of simulation and experimental researches in this field from different perspectives.

Emerging in the 1980s, nonsmooth surface bionic drag reduction has grown rapidly in recent years. Zhu and Zhang [21] built a H-shaped cantilevered structure. Though D-shaped cross section can increase the drag force with the natural resonant vibration frequency, it can strengthen the vortex shedding and the beam deflection. Until now, a square column has been studied the most as the choosing bluff body in galloping piezoelectric energy harvesting. Lim and Lee [22] used wind tunnel tests and flow patterns to study the drag reduction of the flow field around the cylinder on the surface of the convex ring. Wind tunnel tests show that the convex ring on the cylinder (d = 0.0167 D in a pitch interval of 0.165D) can reduce resistance by 9% under the condition that the Reynolds number (Re) is 1.2×10^5 based on the diameter of the cylinder. Wang et al. [23] numerically simulated a concave cylinder with the subcritical Reynolds number (Re = 4×10^4) on nonsmooth cylindrical flow reduction problem. The sensitivity analysis of the structure parameters including the depth, internal shape, and distribution of the pit was also conducted, the results of which show that the concave cylinder has a good drag reduction effect and will work best when h = 0.015 D. The average resistance coefficients of cylindrical concave pit and circular cylinder of diamond distribution pit texture are both 0.923, lower than that of the spherical pit cylinder with 0.94 and that of rectangle with 0.973, respectively. Some scholars have applied the bionic concept to vortex-induced vibration piezoelectric energy harvesting (VIVPEH). Allen and Smits [24] proposed an "eel" shaped flow energy harvester. Experiments were performed to investigate the possibility of using flexible piezoelectric membranes as power generation devices in the ocean. Membranes are excited by the von Kármán vortex street forming behind a bluff body which can transform the flow energy into piezoelectric energy. Bernitsas and his coworkers [25, 26] studied fluid-induced vibrations of smooth cylinders with PTC module, and they divided the galloping into two categories: soft galloping and hard galloping. The former one refers to the gradual increase of the flow velocity when the object is transformed from vortex-induced vibration to galloping by means of self-excitation; the latter one means that the bluff body cannot change from self-excitation to galloping, but it can be converted to galloping by external excitation at a high flow rate. At present, PTC has been successfully applied in VIVACE flow-induced vibration. Based on the morphology of the heterocercal tail of thresher sharks and the ionic polymer-metal composites, Cha et al. [27] designed a bionic fish tail to collect energy from its impact and then proposed a modeling framework for underwater vibration of bionic tail. It is worth mentioning that the feasibility of the model to obtain energy is verified experimentally and theoretically. Akaydin et al. [28] experimentally studied a self-excited energy harvester, which refers to a column attached to the free end of a cantilever beam and partially covered by piezoelectric sheets. The energy harvester is tested in a wind tunnel, generating about 0.1 mW of nonrectified power when the wind speed is 1.192 m/s. The resonant mechanical and electrical efficiency is calculated as 0.72%, while the power of each device is 23.6mW/ m^3, and the piezoelectric volume is 233 W/ m^3. Recently, in order to obtain stronger and more standard eddy current, Pan et al. [29] studied a circular cylinder with an opening and concave surface through experiment and simulation, which simulates two kinds of vortex type systems, respectively, by using two kinds of vortex generator. The results indicate an increase of the induction frequency of the modified cylinder from 2.7 to 2.9 Hz and the peak voltage from 0.35 to 0.41 V. At present, as the derivation direction of vortex-induced vibration with bionic structure becomes more and more diverse, a large number of scholars commit themselves to exploring the nonlinearity [30–33], multi-degree of freedom [34], and multicylinder string juxtaposition [35–37]. To sum up, the bionic structure is indeed a feasible and effective method to improve the bandwidth and output voltage of the energy harvester based on vortex-induced vibration.

In this paper, the VIVPEH characteristics of the bionic cylinder are studied experimentally. In Section 2, the physical and mathematical models of VIVPEH are given. It is noted that the bionic structure model is guaranteed to have the same mass as the corresponding smooth cylinder model. The model verified by experiment in Section 3 is focused on the analysis of the wake oscillator model based on the vortex-induced vibration. The influence of bionic structure model on the performance of harvester is discussed from measuring voltage, bandwidth, and efficiency in Section 4, while the conclusions are given in Section 5.

2. Physical and Mathematical Models

To the best of our knowledge, reducing the resistance in fluid-induced vibration by using the bionic nonsmooth surface structure has been successfully applied in bionic drag reduction technology [38–40]. Based on bionics and mechanical-electric conversion mechanism, the concept of bionics is adopted for the design of bluff body in this paper.

2.1. Physical Model. Many organisms in nature have evolved nonsmooth structures that can help reduce resistance, such as shark scales and the surface of the planthopper's chest. Of course, this pit or convex-clad structure has also been applied to the design of many materials with the golf ball being the most remarkable. As the golf ball moves through the concave structure on the surface, the airflow generates a small vortex near the pit [41]. With the adsorption force of the vortex, the airflow near the sphere begins to move closer to the wall, causing the separation point of the boundary

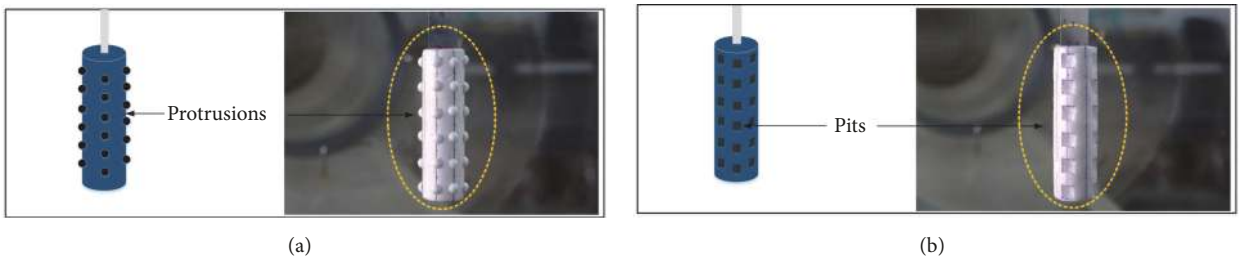

Figure 1: Physical model of bluff bodies with bionic structure. (a) Schematic of the protrusions; (b) schematic of the pits.

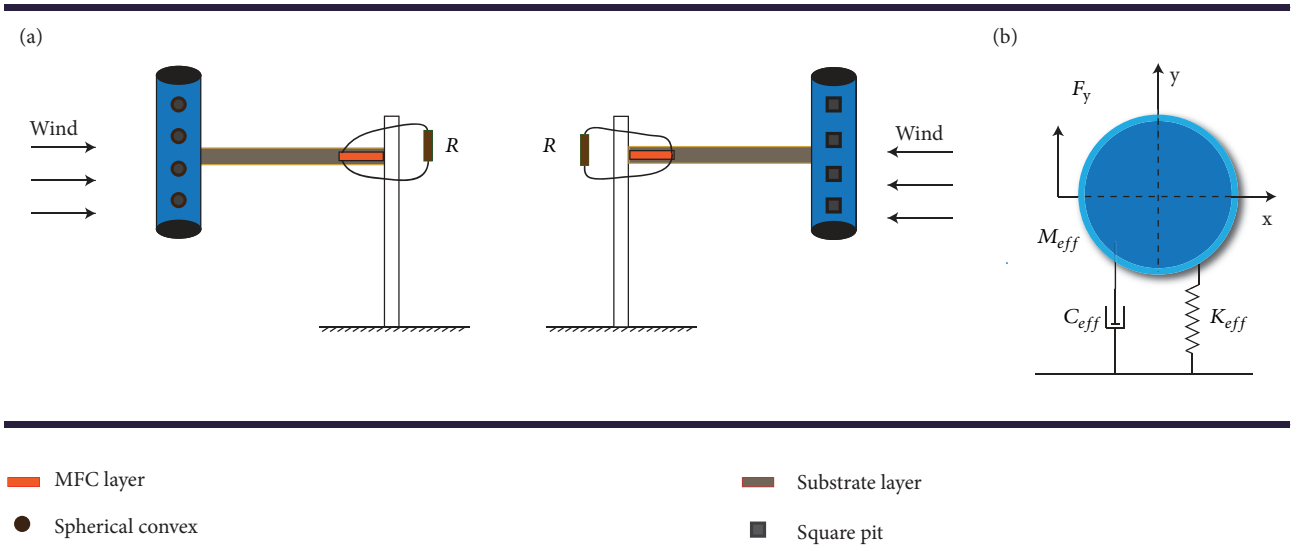

Figure 2: Schematic diagram of VIVPEH with bionic structure: (a) physical diagram in the wind tunnel test; (b) equivalent schematic diagram.

layer to move backward. The vortex area at the rear of the sphere and the pressure difference between the front and the back decline gradually, and so does the pressure difference resistance compared with the smooth sphere. Serving as a bionic structure for fluid vibration experiments in this paper, the size of pits and hemispheric convex is 6 mm, 8 mm, and 10 mm; the number of pits in each smooth cylinder is 3, 4, 5, and 6; and there are twelve bionic structures with pits and hemispheric protrusions, respectively. The physical model is shown in Figure 1.

Based on vortex-induced motions, the mechanism of generating device can be divided into piezoelectric [42–44], electromagnetic, and electrostatic [45–47], among which, piezoelectric type is used and valued the most. Most piezoelectric energy harvesters use a cantilever beam of one or two piezoelectric ceramic layers [48]. The cantilever beam is generally placed on the body of a vibrating structure, and the strain of the piezoelectric layer caused by the vibration can result in an alternating output voltage through the electrode. Figures 2(a) and 2(b) show the schematic diagram of the presented VIVPEH with bionic structure. As shown in Figure 2(a), the wind speed is perpendicular to the cylindrical section, the whole system of which can be simplified as a single degree of freedom system (1DOF). Here, Figure 2(b) can also be called the efficient *M-C-K* vibration system.

In fact, it is feasible to introduce the load resistance into the cantilever energy collection system for equivalent analysis. Besides, another requirement is that the converter is used to adjust the output voltage to maximize the power of the charging and storage device, and to meet the charging demand of small batteries or capacitors [49–51]. For cylinders with bionic structures, it is abstract to study the flow-induced vibration of bluff body directly. Hence, it can be simplified as a mass-spring-damping system on a single degree of freedom.

2.2. Mathematical Model. As shown in Figure 2, there is a cantilever which can vibrate when the bluff body is interacted by the coming wind. As the piezoelectric sheet is coherent in the bottom of the cantilever, a distributed model is used here to simulate the vibration of the cantilever. The distributed parameter model of the energy harvester can be obtained according to the following formula.

$$\ddot{\eta}(t) + 2\zeta\omega_n\dot{\eta}(t) + \omega_n{}^2\eta(t) = F_{VIV}(t) \quad (1)$$

Here $\eta(t)$ is the model coordinate, and the force caused by vortex-induced vibration can be presented as

$$F_{VIV}(t) = 0.25C_{L0}\phi(L)\rho DLU^2 q(t) - 0.5C_D\rho DLU\phi^2(L)\dot{\eta}(t) \quad (2)$$

where C_{L0}, C_D are constants which can be tested by a wind tunnel test, $\phi(x)$ is the model shape function of the cantilever, and $q(t)$ is the variable in the Van Del Pol wake oscillator model for describing the vortex-induced vibration effect which could be determined by

$$\ddot{q}(t) + \varepsilon\omega_f\left[q^2(t) - 1\right]\dot{q}(t) + \omega_f^2 q(t) = \frac{A}{D}\phi(L)\ddot{\eta}(t) \quad (3)$$

where ε and A are also constants which can be tested by wind tunnel test. By adding $\eta(t)\phi(L) = y(t)$, $M_{eff} = 1/\phi^2(L)$, $C_{eff} = 2\zeta\omega_n/\phi^2(L)$,$K_{eff} = \omega_n^2/\phi^2(L)$, the reduced lumped parameter model can be obtained as follows.

$$M_{eff}\ddot{y}(t) + C_{eff}\dot{y}(t) + 0.5C_D\rho DLU\dot{y}(t) + K_{eff}y(t) = 0.25C_{L0}\rho DLU^2 q(t) \quad (4)$$

$$\ddot{q}(t) + \varepsilon\omega_f\left[q^2(t) - 1\right]\dot{q}(t) + \omega_f^2 q(t) = \frac{A}{D}\ddot{y}(t) \quad (5)$$

By adding the electromechanical coupling governing equation:

$$\frac{V(t)}{R} + C_p\dot{V}(t) + \theta\dot{y}(t) = 0 \quad (6)$$

the whole governing equations of the present energy harvesting system could be obtained.

$$\begin{aligned} &M_{eff}\ddot{y}(t) + C_{eff}\dot{y}(t) + 0.5C_D\rho DLU\dot{y}(t) + K_{eff}y(t) - \theta V(t) = 0.25C_{L0}\rho DLU^2 q(t) \\ &\frac{V(t)}{R} + C_p\dot{V}(t) + \theta\dot{y}(t) = 0 \\ &\ddot{q}(t) + \varepsilon\omega_f\left[q^2(t) - 1\right]\dot{q}(t) + \omega_f^2 q(t) = \frac{A}{D}\ddot{y}(t) \end{aligned} \quad (7)$$

Equation (7) is called the concentrated parameter model of nonlinear harvester: M_{eff} and K_{eff} are the equivalent mass; C_{eff} is the system damping, which is related to damping coefficient ζ.K_{eff} is the system equivalent stiffness which depends on the physical properties of the cantilever beam. *y(t)* is the displacement of bluff body vibrating, and *V(t)* is the output voltage. C_P is the capacitance, θ is the piezoelectric coupling coefficient, and *F(t)* is the fluid-dynamical force. It is worth noting that damping coefficient ζ is defined as the ratio of system damping to critical damping, which is expressed as follows.

$$\zeta = \frac{C_{system}}{C_c} = \frac{C_{system}}{2\sqrt{M_{eff}K_{eff}}} \quad (8)$$

The symbol ζ can also be obtained by the free decay experiment. Equation (3) can be rewritten as follows.

$$\zeta = \frac{In\delta}{\sqrt{4\pi^2 + (In\delta)^2}} \quad (9)$$

Here, δ is the ratio of the two adjacent amplitudes in the free decay experiment. Considering the natural frequency $\omega_n = \sqrt{K_{eff}/M_{eff}}$, the system damping C_{system} obtained by the formula is given as below.

$$C_{system} = 2M_{eff}\omega_n\frac{In\delta}{\sqrt{4\pi^2 + (In\delta)^2}} \quad (10)$$

The resistors with different resistance values are connected into the circuit to obtain the optimal load, and the measured data can be used to obtain the open circuit ω_{noc} and short circuit ω_{nsc} frequency by Fourier transform. In this point, the piezoelectric coupling coefficient θ is obtained through the following formula.

$$\theta = \sqrt{\left(\omega_{noc}^2 - \omega_{nsc}^2\right)M_{eff}C_p} \quad (11)$$

Finally, the average power expression $P_{avg} = \int_{U_1}^{U_2}(V_{amplitude}/\sqrt{2})^2/RdU$ is used to obtain the power of harvester, in which V_{max} is the maximum voltage harvested under the maximum tip deflection y_{max}.

3. Experimental Setup and the Theoretical Validation

Figure 3 shows all the instruments needed for this experiment, while the schematic diagram of the bionic structure energy collection system is shown in Figure 1. The entire experiment is implemented in a wind tunnel with the wind speed controlled by frequency conversion device and the conversion relation between frequency and wind speed expressed as $U = 0.137f + 0.18$. The range of wind speed is set at 0 to 7 m/s in the experiment.

The device includes an aluminum cantilever beam with MFC on the root, and the cantilever beam and its column are arranged in "1" shape and placed vertically with a total weight of 5.73 g. With a total length of 168 mm, the cantilever beam is split into two parts which are inserted into the bluff body and exposed to air with a ratio of 0.68 (6.8mm:10mm). The data acquisition instrument is used for signal processing to acquire frequency components. At different wind speeds and resistive loads, a two-channel digital oscilloscope is used to determine the harvester amplitude and peak voltage values. The peak power can be calculated simply from the voltage in the circuit and the corresponding load. In order to ensure the same quality as smooth cylinder, it is essential to have a quality inspection of the cylinder with concave pits and hemispheric convex during the experiment, that is, to add a mass block. The model parameters of concave pits and hemispheric convex are shown in Tables 1 and 2, respectively.

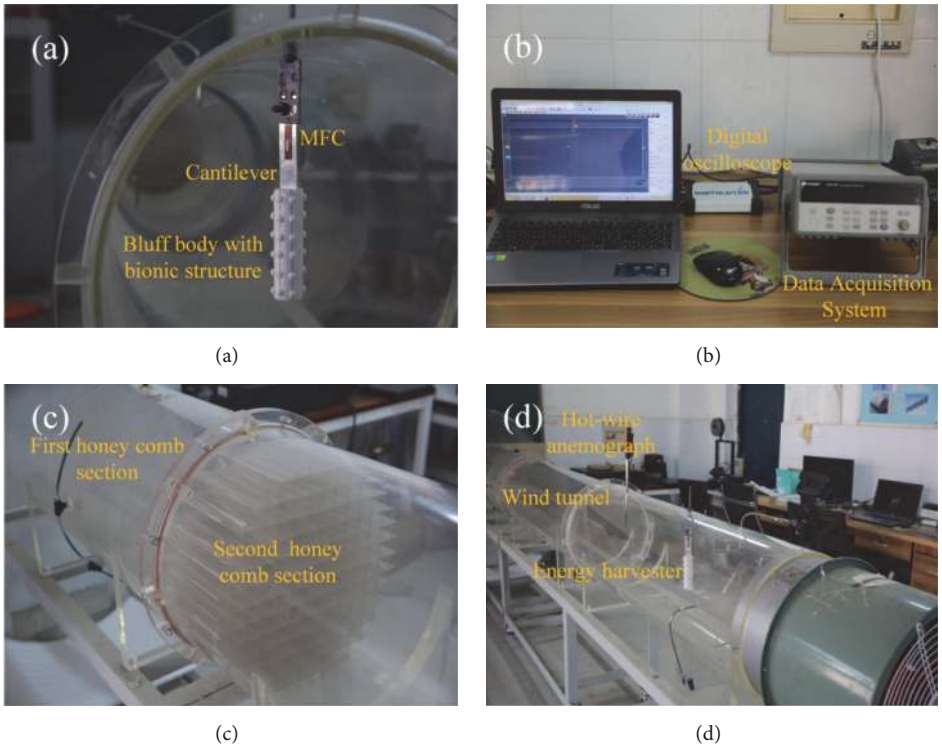

FIGURE 3: Entire experimental setup. (a) The fabricated energy harvester; (b) the data acquisition system; (c) honey comb for air stability; (d) the global views of the wind tunnel.

As is seen in Tables 1 and 2, the maximum mass of the bionic model is 2.48 g and 2.90 g, demonstrating that the mass of other models can be achieved by adding mass blocks. Of course, the same is true for the smooth cylinder. Here, the side length of the pit and the diameter of the hemispherical projection are denoted by L and d, respectively.

Aiming to validate the present aero-electromechanically coupled model, a VIVPEH prototype is prepared and tested in the wind tunnel (Figure 3). The VIVPEH prototype comprises an aluminum cantilever beam bonded with a piezoelectric transducer connected to an electrical load resistance (R_L), and an equilateral smooth cylinder bluff body. The frontal characteristic dimension of the equilateral triangular bluff body is 0.032 m. The identified effective parameters of the VIVPEH are listed in Table 3. Figure 4 shows the comparison of experimental and theoretical results for VIVPEH with smooth cylinder shaped bluff body in an open circuit condition. As shown in Figure 4, in general, the output voltage increases first and then decreases when the wind speed increases. Though the measured data is slightly higher than the theoretical prediction, the theoretical solution and experimental results are generally consistent with each other. The discrepancy is probably attributed to the error caused by the aerodynamic force coefficient of the bluff body. Computed by theoretical method and used in the vortex-induced vibration model, it could be slightly different due to some degree of uncertainty in the experiment. The time history diagrams of peak voltage calculated by

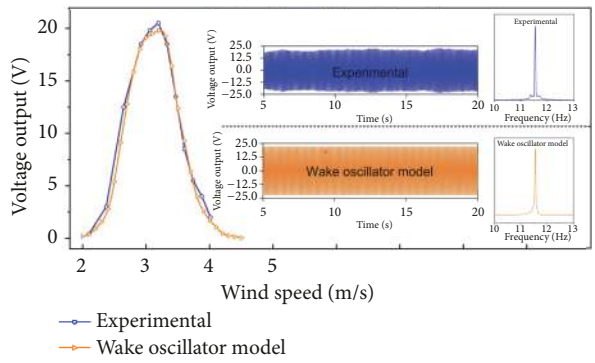

FIGURE 4: Comparison of experimental and theoretical results for VIVPEH with smooth cylinder shaped bluff body.

experiment and theory are shown in the middle of Figure 4, in which the peaks are 20.8 V and 20 V, respectively. On the right is the natural frequency, clearly showing that the experimental result is reasonably close to the theoretical calculating value.

4. Results and Discussions

To highlight the comparison with a smooth cylinder, an experimental analysis on the smooth cylinder is needed. One of the important parameters mentioned in the previous

Table 1: Mass parameters of convex pit models.

Size	3 columns	4 columns	5 columns	6 columns
6mm	2.48g	2.06g	2.16g	2.00g
8mm	2.30g	2.10g	1.91g	2.18g
10mm	2.00g	2.10g	1.91g	2.05g

Table 2: Mass parameters of hemispheric convex models.

Size	3 columns	4 columns	5 columns	6 columns
6mm	2.50g	2.57g	2.51g	2.50g
8mm	2.64g	2.50g	2.55g	2.57g
10mm	2.90g	2.61g	2.60g	2.54g

Table 3: Material parameters involved in the system.

Material parameter	value
Elastic coefficient (K_{eff})(N·m^{-1})	34.07
Capacity (C_p)(nF)	15.7
Active diameter (D_a)(mm)	32
Active height (H)(mm)	118
Active mass (m_c)(g)	2.48/2.90
Equivalent mass (M_{eff})(g)	6.44/6.86
Density (ρ)(kg·m^{-3})	27.38/31.25
System damping (C_{eff})(N·s·m^{-1})	0.0098
Piezoelectric coupling coefficient (θ)(N·V^{-1})	1.183×10^{-5}

section is obtained by the free decay experiment. The natural frequencies ω_n are obtained by the free decay experiment of the smooth cylinder, as shown in Figure 5.

Figure 5(a) shows the time history voltage and displacement: the free decay test of vortex -induced vibration requires initial disturbance to grow until it reaches a locked area and ends up in a stable state. Corresponding to the wave peak, the horizontal coordinate shown as 11.50 Hz is the natural frequency of the system. In order to analyze the influence of bionic structures on the performance of the harvester, the characteristics of smooth, pit, and convex bluff body under different wind speeds and different resistance values are compared in detail, and the resistance values are set as 400 kΩ, 500 kΩ, 600 kΩ, 700 kΩ, 800 kΩ, and 900 kΩ.

4.1. Performance Analysis on Bionic Bluff Body with Pit Shape. The time step curve and the measured voltage under different wind speeds are shown in Figures 6 and 7, respectively. It can be seen from Figure 7 that from three columns to six columns, the voltage rises at first and then declines as the wind speed grows, which verifies the characteristics of VIV; the VIV can be separated into three regions: presynchronization region, lock-in region, and postsynchronization region [52]. Through the overall comparison with the smooth bluff body, the starting vibration wind speed of the bionic structure decreases from 1.8 to 1 m/s, showing that energy can also be harvested at low wind speed. When the size of the square pits on the surface of the cylinder is 6mm, 8mm, and 10mm, the voltage peak also reaches 40, 45, and 47 V, successively, 10 to 15 V higher than that of a smooth cylinder, and the bandwidth also increases from 39.3% to 51.4%. But it is not always suitable to have a bigger or smaller size of the pit for some specific structures, and there is an optimal size. The following is a concrete analysis of each column of pits: in the case of 3 columns, it is obvious that the 10 mm pit has the best vibration effect and plays a reinforcing role in the whole vibration stage with its measured voltage reaching 40 V. In the 4 columns, the voltage curves of the 6 mm and 10mm pits are always above the smooth cylinder, and the bandwidth is also extended. Although the 10 mm pit has an inhibitory effect in the early stage, the voltage in the later stage increases rapidly, even exceeding the voltage values of 6 mm and 10 mm pits. For 5 columns, the 6 mm and 10 mm pits have a weak effect, but the 8 mm pits increase significantly when the wind speed reaches 2.8 m/s. For 6 columns, 8 mm pits show a significant inhibition effect on energy harvesting, and 6mm and 10 mm pits are better than smooth cylinder as the voltage is above 45 V. Therefore, in the engineering field, it is of great significance for the above four models to raise the efficiency of energy collection without increasing the processing materials.

Figures 8(a) and 8(b) are the voltage-wind speed curves of the pit structure and the smooth cylinder, respectively. With

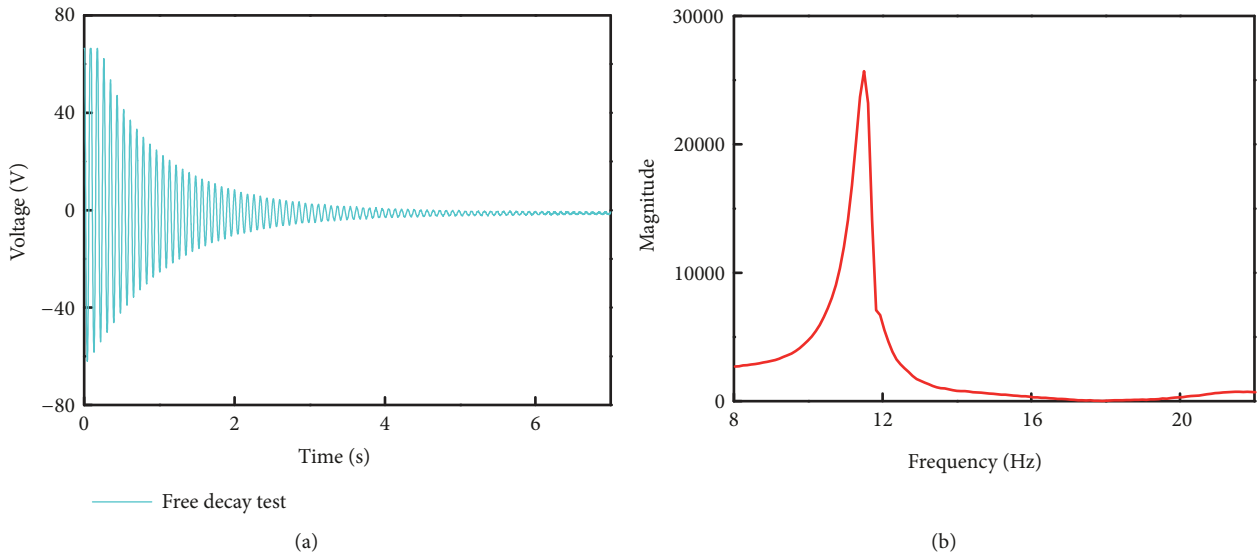

Figure 5: Free decay test of the energy harvester: (a) time history response curve; (b) fast Fourier transforming result.

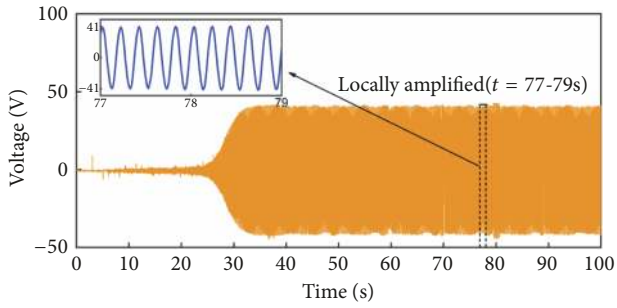

Figure 6: Time history curve of voltage output.

the structure of 4 columns with one side 8mm long selected, it can be seen from Figure 7 that as the wind speed expedites, the voltage and power increase gradually with a constant resistance, but they then descend slowly when reaching their peaks. For the pit structure, the maximum peak voltage is 46 V with a wind speed of 2.92 m/s and a resistance of 900 kΩ, and the maximum peak power is 1.21 mW with a resistance of 800kΩ. The voltage and power begin to decrease when their resistance surpasses 800kΩ. Regardless of voltage or power, the pit structure is higher than the smooth blunt body under the same wind speed and resistance. The optimal resistance measured for the maximum power is 800 kΩ. For the smooth bluff body, the peak voltage is lower than 35 V, about 10 V less than the bionic structure voltage, and the maximum power is only 0.64mW. It can be demonstrated in Figure 8 that the optimal load is around 800 kΩ, which can also be calculated from the time constant in a RC circuit $R_{opt} = 1/\omega_n$. $C_P = 881.5$ kΩ, where ω_n is the natural frequency, and $\omega_n = 2\pi f_n$, $f_n = 11.5$ Hz. It is obvious that the resistance measured is very close to the actual value.

4.2. Performance Analysis on Bionic Bluff Body with Spherical Convex. As it is mentioned in the second section, the convex object model also needs quality inspection, and the quality after verification is 2.90 g. The natural frequency of the vibration changes along with the quality of the bluff body. Therefore, it is also necessary to conduct free decay experiments on the smooth cylinder of 2.90 g and to obtain the natural frequency of the system $f_n = 11.2$ Hz. The output voltage of the bionic structure with different hemispheres of different sizes is measured in the wind tunnel, as shown in Figure 9.

For the 3 columns of convex bionic structure, the hemispherical enhances the amplitude of vortex-induced vibration for the diameter from 6 to 10 mm. Specifically, the output voltage of the 10 mm hemisphere is the largest with its measured voltage close to 50V, 100% higher than that of the smooth cylinder. The enhancement effect is 10 mm>8 mm>6 mm in turn, as shown in Figure 9(a). Figures 9(b) and 9(c) both show strong inhibitory effects, and the measured voltage of the bionic structure is much smaller than that of

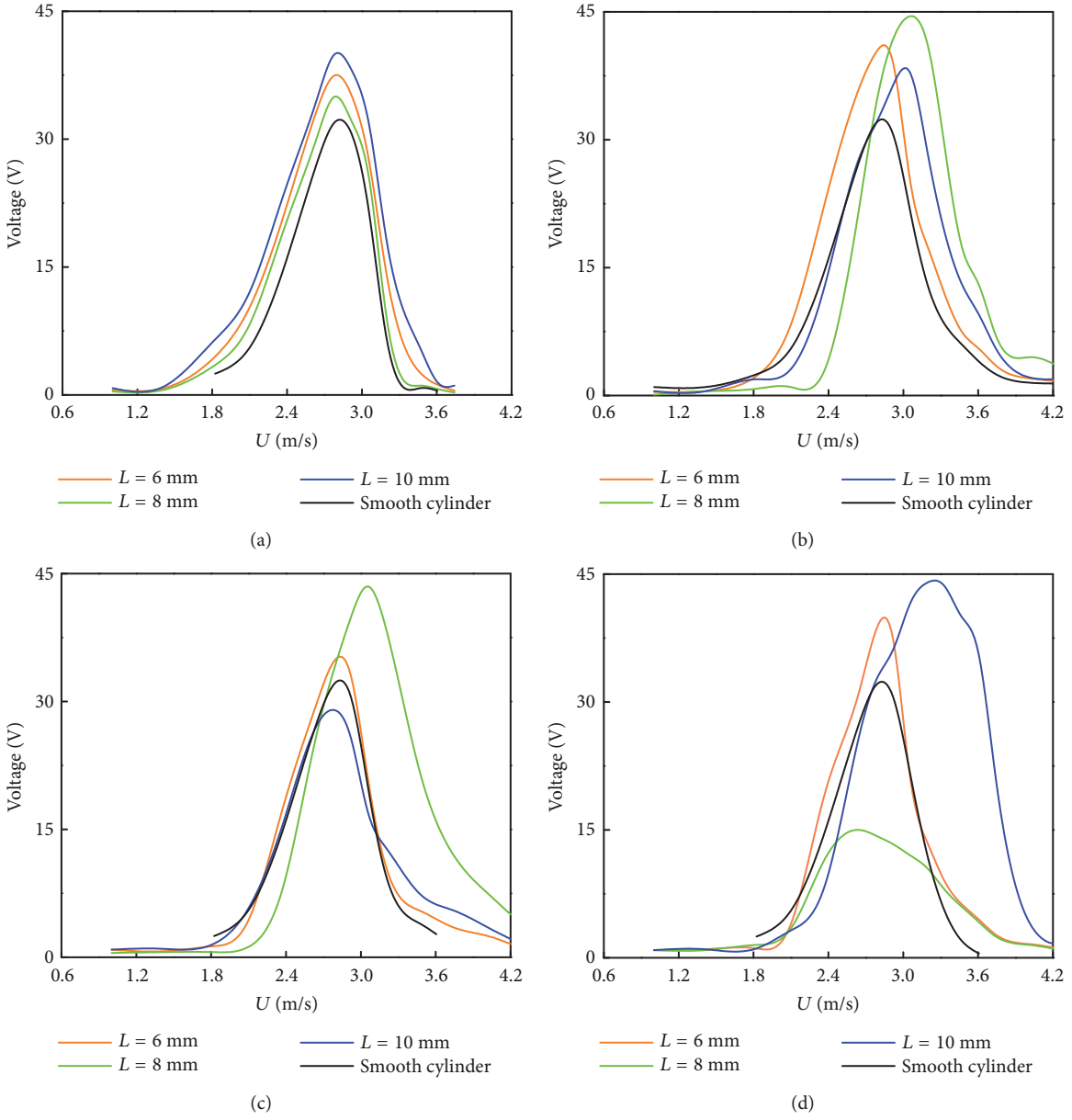

Figure 7: Measured piezoelectric energy harvester data (no resistance): (a) peak voltage versus wind speed of 3 columns of pits; (b) peak voltage versus wind speed of 4 columns of pits; (c) peak voltage versus wind speed of 5 columns of pits; (d) peak voltage versus wind speed of 6 columns of pits.

the smooth cylinder, which means that the 4-column and 5-column hemisphere models have no sense for enhancing the flow-induced vibration. On the contrary, it is of great significance in mitigating the damage of buildings affected by the wind. The relationship between the measured voltage and the wind speed of a 6-column hemispherical bionic cylinder is shown in Figure 9(d). Figure 9(d) shows that 10 mm to 6 mm exhibits different degrees of enhancement or inhibition for flow-induced vibration, but the measured voltage increases first and then decreases as the wind speed accelerates, which is in line with the curve of vortex-induced vibration. In detail, the 10 mm hemisphere acts as reinforcement, and the 6 to 8mm hemisphere suppresses the vibration of the bluff body. Figures 10(a)–10(d) show the power-wind speed curve of two energy harvesting machines, and three columns of 10 mm hemispherical bionic bluff bodies are selected. Figure 10 shows that the threshold wind speed of both energy harvesters is 1.7 m/s. The maximum peak voltage is close to 35 V with a resistance of 800 kΩ and a wind speed of 3.097 m/s. Compared with the smooth structure, the peak power increases from 0.48 to 0.56 mW with the resistance 800 kΩ. Corresponding to the pit model, the optimal load of the hemispheric model is also around 800 kΩ; therefore, it can be considered that the added mass of the hemispheric model is tiny compared with that of the pit model, which can also be verified in Figure 10.

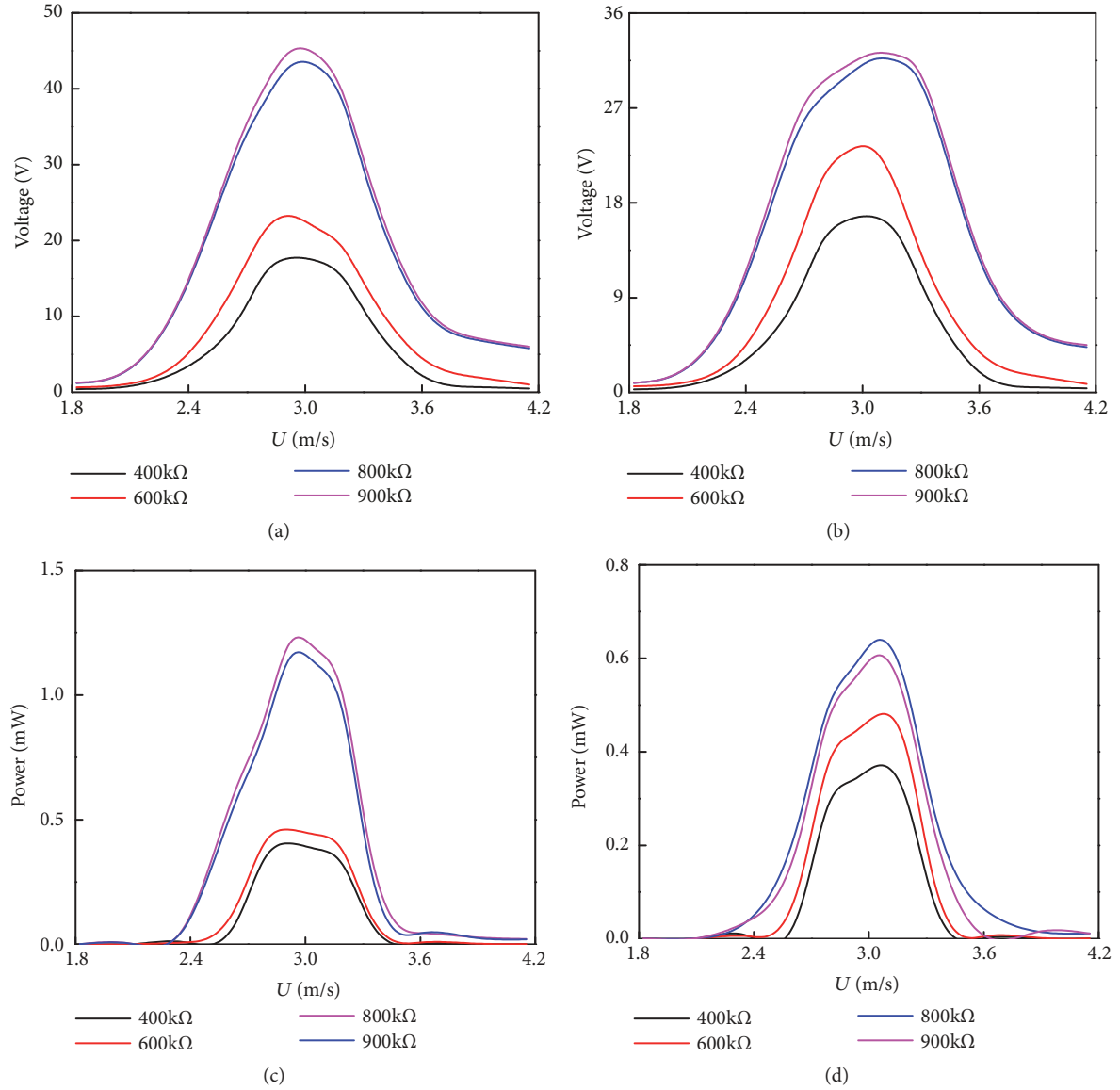

Figure 8: The power-wind and voltage-wind curve of the energy harvester of the pit bionic and smooth structure: (a) the voltage-wind curve of the pit structure; (b) the voltage-wind curve of the smooth cylinder; (c) the power-wind curve of the pit structure; (d) the power-wind curve of the smooth cylinder.

5. Conclusions

The piezoelectric energy harvesting characteristics of smooth cylinders with pits and hemispherical protrusions are comprehensively evaluated by experimental methods. The relationship between maximum voltage and resonance frequencies of each model under different wind speeds is studied under the condition of the same equivalent mass. The experimental result demonstrates an effect on the performance of the harvester exerted by the size and distribution of the square pit and hemispherical convex hull. In terms of the pit structure, the locking area is concentrated on 2 to 3.5 m/s. The 6 to 10mm square pit can reduce the threshold wind speed; meanwhile, it has a different effect on the enhancement of vibration, which is closely related to the number of pit columns. For example, the measured voltage of 4 columns and 5 columns of 8 mm pits can reach about 47 V, while the voltage of 6 columns of 8 mm pits is much lower than that of the smooth cylinders. As for convex structures, the 10 mm hemispherical convex structures of 3 columns and 6 columns have excellent effects on increasing amplitude of vibration, according to the piezoelectric principle; namely, the higher the amplitude is, the higher the measuring voltage will be. The measured voltage is close to 50 V, completely higher than that of the smooth cylinder. The power output of 10 mm convex structure is 0.56 mW, slightly higher than the smooth cylinder under the same conditions. On the contrary, 4-column and 5-column hemispheric convex

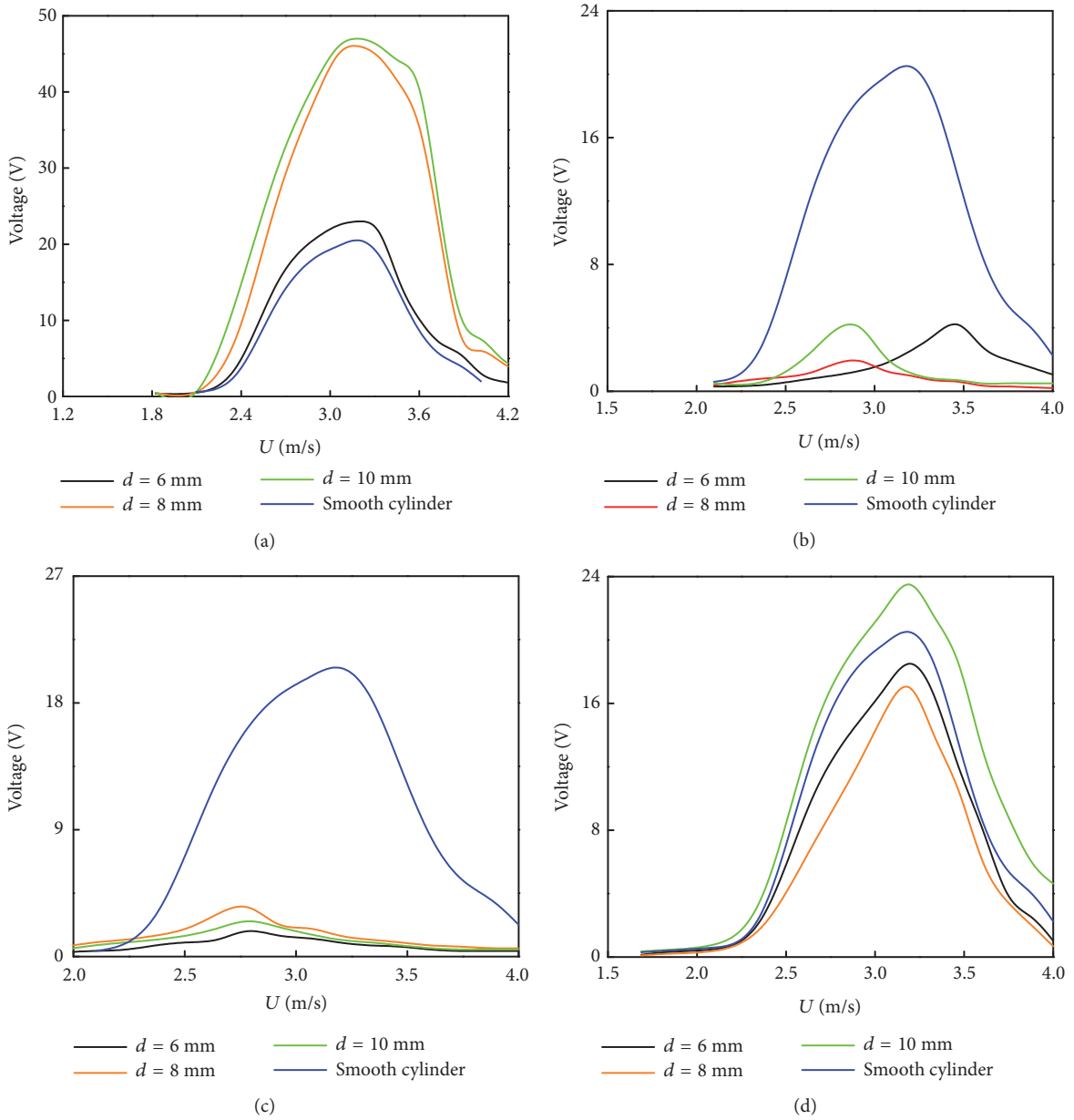

Figure 9: Measured piezoelectric energy harvester data (no resistance): (a) peak voltage versus wind speed of 3-column hemisphere protrusion; (b) peak voltage versus wind speed of 4-column hemisphere protrusion; (c) peak voltage versus wind speed of 5-column hemisphere protrusion; (d) peak voltage versus wind speed of 6-column hemisphere protrusion.

structures have obvious inhibiting effects on the flow-induced vibration of bluff body, which can be used for vibration reduction. For wind tunnel experiments with load resistance, the measured voltage increases with the load resistance, and the optimal load of both bionic energy collection systems is around 800 kΩ. In summary, the bionic structure energy harvesting system design can serve as a good method to obtain high voltage from wind-induced vibration. Finally, it should be mentioned that the parametric study is performed for our present bionic structures. A comparison to other methods and more efficient bionic structures for improving performance will be further studied in the future work.

Data Availability

The data sets used to support the findings of this study are included within the article.

Conflicts of Interest

The authors declare that they have no conflicts of interest.

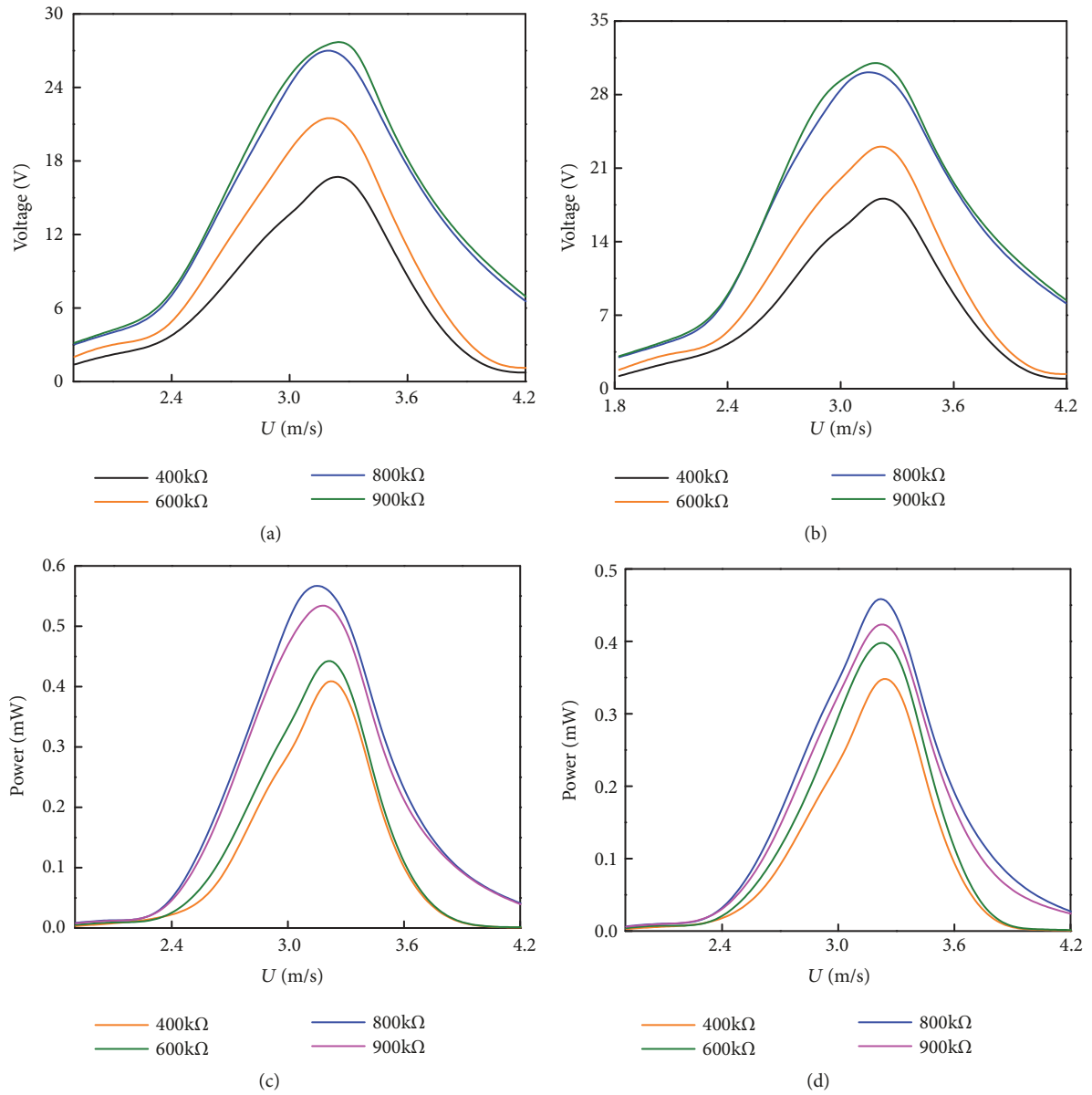

FIGURE 10: Comparison of voltage and power response between smooth cylinder and hemisphere protrusion structure: (a) voltage response of smooth cylinder; (b) voltage response of hemisphere; (c) power response of hemisphere protrusion structure; (d) power response of smooth cylinder structure.

Acknowledgments

We gratefully appreciate the financial support for this project from the National Natural Science Foundation of China (Nos. 21676257 and 51606171).

References

[1] L. Yu and Y. P. Li, "A flexible-possibilistic stochastic programming method for planning municipal-scale energy system through introducing renewable energies and electric vehicles," *Journal of Cleaner Production*, vol. 207, pp. 772–787, 2019.

[2] S. F. Tang, D. L. Yuan, and Y. D. Rao, "Percarbonate promoted antibiotic decomposition in dielectric barrier discharge plasma," *Journal of Hazardous Materials*, vol. 366, pp. 669–676, 2019.

[3] Z. E. Zhang, Y. F. Li, W. X. Zhang, J. L. Wang, M. R. Soltanian, and A. G. Olabi, "Effectiveness of amino acid salt solutions in capturing CO2: A review," *Renewable & Sustainable Energy Reviews*, vol. 98, pp. 179–188, 2018.

[4] Q. N. Sun, Y. J. Yang, Z. X. Zhao et al., "Elaborate design of polymeric nanocomposites with Mg(ii)-buffering nanochannels for highly efficient and selective removal of heavy metals from water: case study for Cu(ii)," *Environmental Science: Nano*, vol. 5, no. 10, pp. 2440–2451, 2018.

[5] H. Li, L. Luo, P. Kunal et al., "Oxygen Reduction Reaction on Classically Immiscible Bimetallics: A Case Study of RhAu," *The Journal of Physical Chemistry C*, vol. 122, no. 5, pp. 2712–2716, 2018.

[6] G. Yang, J. Wang, H. W. Zhang, H. Jia, Y. Zhang, and F. Gao, "Applying bio-electric field of microbial fuel cell-upflow anaerobic sludge blanket reactor catalyzed blast furnace dusting ash for promoting anaerobic digestion," *Water Research*, vol. 149, pp. 215–224, 2019.

[7] H. Li, K. Shin, and G. Henkelman, "Effects of ensembles, ligand, and strain on adsorbate binding to alloy surfaces," *The Journal of Chemical Physics*, vol. 149, no. 17, Article ID 174705, 8 pages, 2018.

[8] C. W. Duan, Y. Z. Cao, L. X. Hu, D. Fu, and J. L. Ma, "Synergistic effect of TiF3 on the dehydriding property of a-AlH3 nanocomposite," *Materials Letters*, vol. 238, pp. 254–257, 2019.

[9] K. Wang, S. Z. Zhou, Y. T. Zhou, J. Ren, L. W. Li, and Y. Lan, "Synthesis of Porous Carbon by Activation Method and its Electrochemical Performance," *International Journal of Electrochemical Science*, pp. 10766–10773, 2018.

[10] Y. L. Hou, Y. Tie, C. Li, T. Sapanathan, and M. Rachik, "Low-velocity impact behaviors of repaired CFRP laminates: Effect of impact location and external patch configurations," *Composites Part B: Engineering*, vol. 163, pp. 669–680, 2019.

[11] K. P. Wu, K. Du, and G. R. Hu, "A novel design concept for fabricating 3D graphene with the assistant of anti-solvent precipitated sulphates and its Li-ion storage properties," *Journal of Materials Chemistry A*, vol. 6, no. 8, pp. 3444–3453, 2018.

[12] K. P. Wu, D. W. Liu, and Y. Tang, "In-situ single-step chemical synthesis of graphene-decorated CoFe2O4 composite with enhanced Li ion storage behaviors," *Electrochimica Acta*, vol. 263, pp. 515–523, 2018.

[13] C. X. Duan, J. B. Huo, F. E. Li, M. H. Yang, and H. X. Xi, "Ultrafast room-temperature synthesis of hierarchically porous metal–organic frameworks by a versatile cooperative template strategy," *Journal of Materials Science*, vol. 53, no. 24, pp. 16276–16287, 2018.

[14] L. Kang, H. L. Du, H. Zhang, and W. L. Ma, "Systematic research on the application of steel slag resources under the background of big data," *Complexity*, 2018.

[15] K. J. Yu, B. Y. Qu, and C. T. Yue, "A performance-guided JAYA algorithm for parameters identification of photovoltaic cell and module," *Applied Energy*, vol. 237, pp. 241–257, 2019.

[16] K. Yin, S. Yang, X. R. Dong, D. K. Chu, X. Gong, and J. A. Duan, "Femtosecond laser fabrication of shape-gradient platform: underwater bubbles continuous self-driven and unidirectional transportation," *Applied Surface Science*, vol. 471, pp. 999–1004, 2019.

[17] Y. L. Zhang, Y. S. Hu, X. G. Guo, and F. Wang, "Micro Energy Harvester With Dual Electrets on Sandwich Structure Optimized by Air Damping Control for Wireless Sensor Network Application," *IEEE Access*, vol. 6, pp. 26779–26788, 2018.

[18] J. L. Wang, L. H. Tang, L. Y. Zhao, and Z. E. Zhang, "Efficiency investigation on energy harvesting from airflows in HVAC system based on galloping of isosceles triangle sectioned bluff bodies," *Energy*, vol. 172, pp. 1066–1078, 2019.

[19] J. L. Wang, G. P. Li, M. Zhang et al., "Energy harvesting from flow-induced vibration: a lumped parameter model," *Energy Sources, Part A: Recovery, Utilization, and Environmental Effects*, vol. 40, no. 24, pp. 2903–2913, 2018.

[20] J. L. Wang, S. X. Zhou, Z. E. Zhang, and D. Yurchenko, "High-performance piezoelectric wind energy harvester with Y-shaped attachments," *Energy Conversion and Management*, vol. 181, pp. 645–652, 2019.

[21] J. Zhu and W. Zhang, "Coupled analysis of multi-impact energy harvesting from low-frequency wind induced vibrations," *Smart Materials and Structures*, vol. 24, no. 4, Article ID 045007, 2015.

[22] H. C. Lim and S. J. Lee, "Flow control of a circular cylinder with O-rings," *Fluid Dynamics Research*, vol. 35, no. 2, pp. 107–122, 2004.

[23] G. R. Wang, C. J. Liao, G. Hu, L. Zhong, and M. Zhang, "Numerical simulation analysis and the drag reduction performance investigation on circular cylinder with dimples at subcritical reynolds number," *Jixie Qiangdu/Journal of Mechanical Strength*, vol. 39, no. 5, pp. 1119–1125, 2017.

[24] J. J. Allen and A. J. Smits, "Energy harvesting EEL," *Journal of Fluids and Structures*, vol. 15, no. 3-4, pp. 629–640, 2001.

[25] H. Park, R. A. Kumar, and M. M. Bernitsas, "Enhancement of flow-induced motion of rigid circular cylinder on springs by localized surface roughness at 3×10^4 ≤Re≤1. 2×10^5," *Ocean Engineering*, vol. 72, pp. 403–415, 2013.

[26] E. S. Kim, M. M. Bernitsas, and R. A. Kumar, "Multicylinder flow-induced motions: enhancement by passive turbulence control at 28,000<Re<120,000," *Journal of Offshore Mechanics and Arctic Engineering*, vol. 135, no. 2, Article ID 021802, 2013.

[27] Y. Cha, M. Verotti, H. Walcott, S. D. Peterson, and M. Porfiri, "Energy harvesting from the tail beating of a carangiform swimmer using ionic polymer-metal composites," *Bioinspiration & Biomimetics*, vol. 8, no. 3, Article ID 036003, 2013.

[28] H. D. Akaydin, N. Elvin, and Y. Andreopoulos, "The performance of a self-excited fluidic energy harvester," *Smart Materials and Structures*, vol. 21, no. 2, Article ID 025007, 2012.

[29] F. F. Pan, Z. K. Xu, P. Pan, and L. Jin, "Piezoelectric energy harvesting from vortex-induced vibration using a modified circular cylinder," in *Proceedings of the International Conference on Electrical Machines and Systems*, pp. 1–5, 2017.

[30] S. X. Zhou and L. Zuo, "Nonlinear dynamic analysis of asymmetric tristable energy harvesters for enhanced energy harvesting," *Communications in Nonlinear Science and Numerical Simulation*, vol. 61, pp. 271–284, 2018.

[31] S. X. Zhou, J. Y. Cao, D. J. Inman, J. Lin, S. S. Liu, and Z. Z. Wang, "Broadband tristable energy harvester: modeling and experiment verification," *Applied Energy*, vol. 133, pp. 33–39, 2014.

[32] D. M. Huang, S. X. Zhou, and G. Litak, "Theoretical analysis of multi-stable energy harvesters with high-order stiffness terms," *Communications in Nonlinear Science and Numerical Simulation*, vol. 69, pp. 270–286, 2019.

[33] M. H. Yao, Y. Niu, and Y. X. Hao, "Nonlinear dynamic responses of rotating pretwisted cylindrical shells," *Nonlinear Dynamics*, vol. 95, no. 1, pp. 151–174, 2019.

[34] S. X. Zhou, J. D. Hobeck, J. Y. Cao, and D. J. Inman, "Analytical and experimental investigation of flexible longitudinal zigzag structures for enhanced multi-directional energy harvesting," *Smart Materials and Structures*, vol. 26, no. 3, Article ID 035008, 2017.

[35] S. X. Zhou and J. L. Wang, "Dual serial vortex-induced energy harvesting system for enhanced energy harvesting," *AIP Advances*, no. 7, Article ID 075221, 2018.

[36] K. Muralidharan, S. Muddada, and B. S. V. Patnaik, "Numerical simulation of vortex induced vibrations and its control by suction and blowing," *Applied Mathematical Modelling*, vol. 37, no. 1-2, pp. 284–307, 2013.

[37] J. L. Wang, L. F. Geng, M. Zhang et al., "Broadening band of wind speed for aeroelastic energy scavenging of a cylinder through buffeting in the wakes of a squared prism," *Shock and Vibration*, vol. 2018, 2018.

[38] L. M. Tian, L. Q. Ren, Q. P. Liu, Z. W. Han, and X. Jiang, "The mechanism of drag reduction around bodies of revolution using bionic non-smooth surfaces," *Journal of Bionic Engineering*, vol. 4, no. 2, pp. 109–116, 2007.

[39] Y. Q. Gu, G. Zhao, J. X. Zheng, Z. Y. Li, W. B. Liu, and F. K. Muhammad, "Experimental and numerical investigation on drag reduction of non-smooth bionic jet surface," *Ocean Engineering*, vol. 81, pp. 50–57, 2014.

[40] J. L. Wang, G. F. Zhao, M. Zhang, and Z. E. Zhang, "Efficient study of a coarse structure number on the bluff body during the harvesting of wind energy," *Energy Sources, Part A: Recovery, Utilization, and Environmental Effects*, vol. 40, no. 15, pp. 1788–1797, 2018.

[41] S. K. Kumar, C. Bose, S. F. Ali, S. Sarkar, and S. Gupta, "Investigations on a vortex induced vibration based energy harvester," *Applied Physics Letters*, vol. 111, no. 24, Article ID 243903, 2017.

[42] L. C. Zhao, H. X. Zou, G. Yan et al., "A water-proof magnetically coupled piezoelectric-electromagnetic hybrid wind energy harvester," *Applied Energy*, vol. 239, pp. 735–746, 2019.

[43] X. F. He, X. K. Yang, and S. L. Jiang, "Enhancement of wind energy harvesting by interaction between vortex-induced vibration and galloping," *Applied Physics Letters*, vol. 112, no. 3, Article ID 033901, 2018.

[44] M. Zhang and J. L. Wang, "Experimental study on piezoelectric energy harvesting from vortex-induced vibrations and wake-induced vibrations," *Journal of Sensors*, vol. 2016, 2016.

[45] X. Q. Zhao, J. Cai, Y. Guo, C. B. Li, J. L. Wang, and H. W. Zheng, "Modeling and experimental investigation of an AA-sized electromagnetic generator for harvesting energy from human motion," *Smart Material and Structures*, vol. 27, no. 8, Article ID 085008, 2018.

[46] P. D. Mitcheson, T. C. Green, and E. M. Yeatman, "Power processing circuits for electromagnetic, electrostatic and piezoelectric inertial energy scavengers," *Microsystem Technologies*, vol. 13, no. 11-12, pp. 1629–1635, 2007.

[47] T. N. Kato and H. Takabe, "Electrostatic and electromagnetic instabilities associated with electrostatic shocks: Two-dimensional particle-in-cell simulation," *Physics of Plasmas*, vol. 17, no. 3, Article ID 032114, 2010.

[48] H. C. Liu, J. W. Zhong, C. K. Lee, S. W. Lee, and L. W. Lin, "A comprehensive review on piezoelectric energy harvesting technology: Materials, mechanisms, and applications," *Applied Physics Reviews*, vol. 5, no. 5, Article ID 041306, 2018.

[49] S. X. Zhou, J. Y. Cao, A. Erturk, and J. Lin, "Enhanced broadband piezoelectric energy harvesting using rotatable magnets," *Applied Physics Letters*, vol. 102, no. 17, Article ID 173901, 2013.

[50] G. B. Hu, L. H. Tang, and R. Das, "Internally coupled metamaterial beam for simultaneous vibration suppression and low frequency energy harvesting," *Journal of Applied Physics*, vol. 123, no. 5, Article ID 055107, 2018.

[51] Z. S. Chen, J. He, J. H. Liu, and Y. P. Xiong, "Switching delay in self-powered nonlinear piezoelectric vibration energy harvesting circuit: mechanism, effects and solution," *IEEE Transactions on Power Electronics*, vol. 34, no. 3, pp. 2427–2440, 2019.

[52] J. L. Wang, J. Y. Ran, and Z. E. Zhang, "Energy harvester based on the synchronization phenomenon of a circular cylinder," *Mathematical Problems in Engineering*, vol. 2014, 2014.